EASR

Engineering and Applied Science Research

https://www.tci-thaijo.org/index.php/easr/index

Published by the Faculty of Engineering, Khon Kaen University, Thailand

Effect of active layer thickness on the performance of amorphous hydrogenated silicon solar cells

Soni Prayogi*[1, 2], Yoyok Cahyono[1], Dadan Hamdani[1, 3] and Darminto*[1]

[1]Advanced Materials Research Group, Department of Physics, Institut Teknologi Sepuluh Nopember, Surabaya 60111, Indonesia
[2]Department of Physics, Syiah Kuala University, Banda Aceh 23111, Indonesia
[3]Department Physics Study Program, FMIPA, Mulawarman University, Samarinda 75117, Indonesia

Received 15 December 2020
Revised 5 June 2021
Accepted 11 June 2021

Abstract

Hydrogenated amorphous silicon (a-Si: H) materials have received a great deal of attention for their potential to make inexpensive solar cells. In this work, we report that the effect of adding active layers in the a-Si: H p-i-n to p-i_1-i_2-n solar cell structure greatly affects the increase in conversion efficiency. Solar cells a-Si: H p-i_1-i_2-n were grown using the *Plasma Enhanced Chemical Vapor Deposition* (PECVD) technique on *Indium Tin Oxide* (ITO) substrate. The ITO substrate used for transparency and conductivity properties are superior among other oxide materials. The a-Si: H p-i_1-i_2-n solar cells were characterized including optical properties, electrical properties, energy gap using *Spectroscopic Ellipsometric* (SE), surface morphology using *Atomic Force Microscopy* (AFM) and solar cell performance (I-V curve) measured using solar simulator. The structure of solar cells a-Si: H p-i_1-i_2-n functions to capture sunlight energy that is not captured by the first intrinsic layer and can then be captured by the second intrinsic layer. Our results show that there is a very good increase from 7.79% in the p-i_1-i_2-n sample to 8.49% in the p-i_2-i_1-n sample.

Keywords: Solar cells, a-Si: H, p-i_1-i_2-n, p-i_2-i_1-n, PECVD

1. Introduction

One of the main problems found in hydrogenated amorphous silicon (a-Si: H) based solar cells is the instability of their efficiency after being exposed to high intensity for a long period of time. This phenomenon is known as the *Staebler-Wronski Effect* (SWE) [1-3]. The high hydrogen content is then known as one of the causes of SWE, where the silicon-hydrogen bond is easily released by the influence of high-intensity irradiation, leaving defects in the solar cell material [4, 5]. Therefore, several researchers then developed the *Plasma Enhanced Chemical Vapor Deposition* (PECVD) technique to overcome this problem. Material a-Si: H grown with PECVD by utilizing plasma as a growing medium [6, 7]. This technique uses Silan gas (SiH_4) as the source gas, which is 10% in Hydrogen (H_2) gas and an amorphous silicon material with a hydrogen content of 10-20% is obtained [8].

Increasing the efficiency of hydrogenated amorphous silicon (a-Si: H) based solar cells, especially to optimize the quality of the thin film on the p-i-n part of the solar cell, this part is the main part to convert solar energy into electrical energy [9, 10]. If the quality in the manufacture of this thin layer of p-i-n solar cells is good, the efficiency of solar cells can increase between 5-21% [11, 12]. Meanwhile, the concentration of boron or phosphorus dopants can affect the type of thin layer formed, so that the electron and hole concentrations can be controlled [13, 14]. The use of ITO is often used in solar cell applications because it has high stability against photo-corrosion, the price is relatively cheap and does not cause harmful effects to health and the environment. Usually the energy gap width in p-i-n solar cells also greatly affects the magnitude of the conversion efficiency of solar cells, it is also required to have a high absorption rate so that the photovoltaic effect obtained can be optimum [15].

In this work, we reported the characteristics of hydrogenated amorphous silicon (a-Si: H) based solar cells with the addition of an active layer (i-layer). As we know, i-layer of the a-Si: H-based p-i-n solar cell device plays the most important role in the utilization of photon energy to excite its charge carrier from the valence band to the conduction band [16]. Furthermore, more photons will be absorbed if the active layer is thicker so that the charge carrier generation rate increases. On the other hand, the thicker i-layer also contributes to an increase in the localized state as well as an increase in the series resistance, thereby reducing the conversion efficiency of the solar cell [17, 18]. Therefore, the addition of the active layer (i-layer) with the optimum thickness will provide the best characteristics directly by maintaining the quality of the material, which is indirectly related to the technique used when growing the material. In this fabrication, we make an atempt for an approach by employing double active layers in producing junction having the structure of p-i_1-i_2-n, where each i layer has different band energy gap.

*Corresponding author.
Email address: prayogi.sp@gmail.com; darminto@physics.its.ac.id
doi: 10.14456/easr.2022.22

2. Materials and methods

The deposition of intrinsic double layer solar cells p-i_1-i_2-n a-Si: H was carried out using *Radio Frequency-Plasma Enhanced Chemical Vapor Deposition* (RF-PECVD) (MVSystem Inc. USA), as shown in Figure 1. Plasma is formed through inelastic collisions between gas molecules and electrons in the discharge chamber. An electric field to accelerate electrons was supplied an AC voltage with a frequency of 13.56 MHz (RF) [19]. Hydrogen and silane gases flowed through a pipeline into the chamber, decomposed into neutral reactive species (SiH, SiH_2, SiH_3, Si_2H_6, H, H_2, etc.), and were converted to positively charged ions (H^+, SiH^+, SiH_2^+, and SiH_3^+) [20]. Atomic force microscopy (AFM) measurements were performed using an instrument manufactured by AIST-NT (Smart SPM 1000). The instrument was used in tapping mode on a scanned area of 1 μm by 1 μm. The AFM images were evaluated applying several features of the Gwyddion software79 including data leveling, background subtraction and false color mapping. Surface roughness value *Root-Mean-Square (RMS)*:

$$\mathrm{RMS} = \sqrt{\frac{1}{l_r}\int_0^{l_r} z(x)^2 dx}. \quad (1)$$

To get the double intrinsic layer made by diluting silane plasma by hydrogen, with the ratio of hydrogen and silane, R= H_2/SiH_4 was varied energy band gap for a-Si: H films deposited with hydrogen dilution of R = 0, R = 16, and 36 [21], while the extrinsic layer of n-type and n-type was fixed for each sample. Furthermore, the sample is in the metal layer on the back which acts as an electrical contact and a light reflector. Deposition parameters can be seen in Table 1 and Table 2 with the hope that it can also produce good quality solar cell efficiency. At each layer, characterization is carried out or physical properties are searched, namely thickness morphology, optical properties, band gap, electrical properties using *Spectroscopic Ellipsometric* (SE) UVISEL-Horiba and I-V characterization of intrinsic double layer solar cells p-i_1-i_2-n a-Si: H with solar simulator *Keithley 617*.

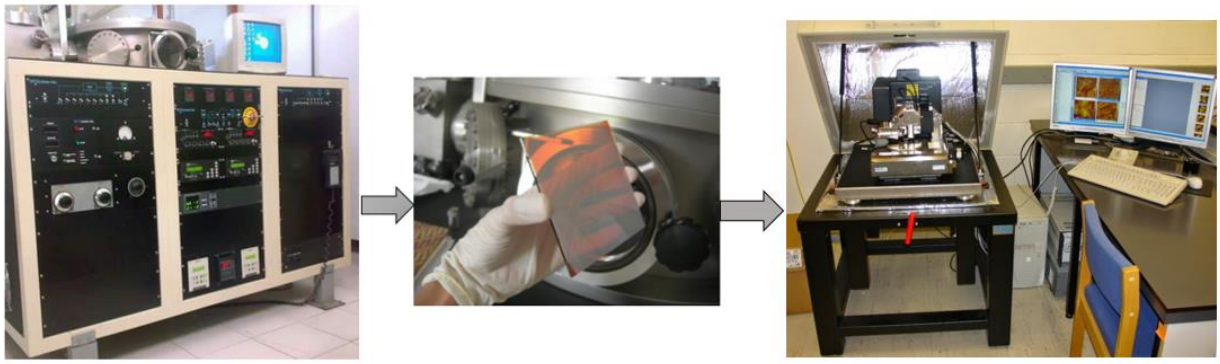

(a) (b) (c)

Figure 1 Scheme of solar cells a-Si: H deposition of sample p-i_1-i_2-n and sample p-i_2-i_1-n (a) system with multi-chamber RF-PECVD (MVSystem Inc. USA). (b) The samples of solar cells a-Si: H (10x10) cm^2 integrated with the conductive film, and (c) *Atomic Force Microscopy* (AFM) AIST-NT (Smart SPM 1000).

Table 1 Solar cells a-Si: H sample p-i_1-i_2-n deposition parameters.

Sample	Type	Forming parameters		*Eg*	Thickness
p-i_1-i_2-n	p	S_iH_4	20 sccm	2.04 eV	35 nm
		B_2H_6	2 sccm		
		H_2	40 sccm		
		Power RF	5 Watt		
		Temperature	210ºC		
		Pressure	4800 mTorr		
		Time	10 Minute		
	i_1	R (H_2/S_iH_4)	0	1.92 eV	200 nm
		Power RF	10 Watt		
		Temperature	270ºC		
		Pressure	2000 mTorr		
		Time	140 Minute		
	i_2	R (H_2/S_iH_4)	16	1.66 eV	400 nm
		Power RF	10 Watt		
		Temperature	270ºC		
		Pressure	2000 mTorr		
		Time	90 Minute		
	n	S_iH_4	20 sccm	2.19 eV	65 nm
		PH_4	5 sccm		
		H_2	20 sccm		
		Power RF	5 Watt		
		Temperature	210ºC		
		Pressure	5300 mTorr		
		Time	10 Minute		

Table 2 Solar cells a-Si: H sample p-i_2-i_1-n deposition parameters.

Sample	Type	Forming parameters		*Eg*	Thickness
p-i_2-i_1-n	**p**	S_iH_4	20 sccm	2.04 eV	35 nm
		B_2H_6	2 sccm		
		H_2	40 sccm		
		Power RF	5 Watt		
		Temperature	210°C		
		Pressure	4800 mTorr		
		Time	10 Minute		
	i_2	R (H_2/S_iH_4)	16	1.66 eV	400 nm
		Power RF	10 Watt		
		Temperature	270°C		
		Pressure	2000 mTorr		
		Time	90 Minute		
	i_1	R (H_2/S_iH_4)	0	1.92 eV	200 nm
		Power RF	10 Watt		
		Temperature	270°C		
		Pressure	2000 mTorr		
		Time	140 Minute		
	n	S_iH_4	20 sccm	2.19 eV	65 nm
		PH_4	5 sccm		
		H_2	20 sccm		
		Power RF	5 Watt		
		Temperature	210°C		
		Pressure	5300 mTorr		
		Time	10 Minute		

3. Results and discussion

The SE technique was used to characterize a-Si: H, hydrogenated nano-crystalline silicon (nc-Si: H) and hydrogenated crystal microstructure (μc-Si: H) prepared by RF-PECVD. The transition from amorphous phase to nc/μc-Si: H can be identified qualitatively by in-situ and ex-situ SE techniques [21-24]. This work has also been used to study the diffusion of hydrogen into films and the kinetics of hydrogen interaction with a-Si: H during plasma H_2 treatment. It is possible to determine optical constants, bandgaps, thickness, amorphous fraction, crystals and cavities, surface layer thickness through dielectric function analysis using suitable models namely Tauc-lorentz (TL) and Bruggman effective medium approximation model (BEMA).

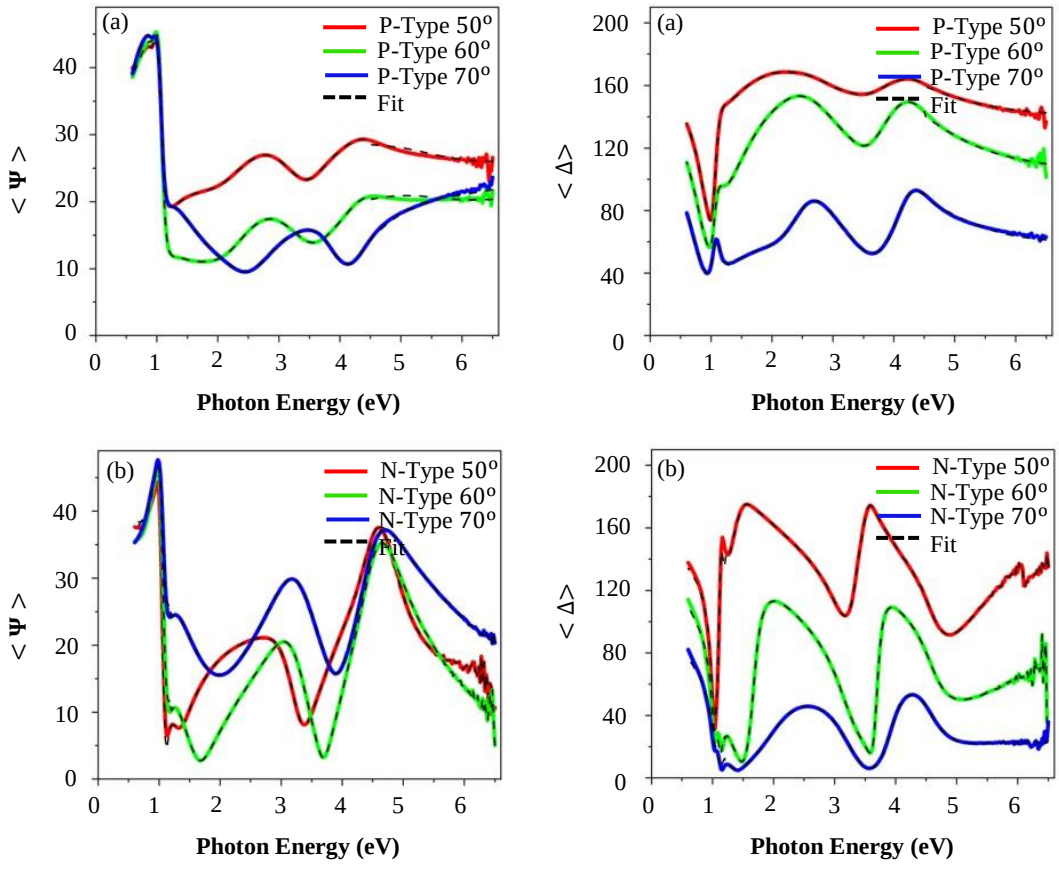

Figure 2 Real and imaginary part fitting model (a) p-type and (b) n-type of the values of ψ and Δ measured in SE with an angle of 50°, 60° and 70°

Measurement <ψ> and <Δ> of SE to layers p-type and n-type shown in Figure 2, layers i_1-type and i_2-type shown in Figure 3 along with the results of data fitting. The dielectric function <ε> describes the optical and electrical properties of the material over the measurement energy range. The dielectric function consists of two components, namely real <ε_1> and imaginary <ε_2>. The real component <ε_1> represents the polarization of the material due to the electric dipole which contributes to the atomic and electric polarization, while the imaginary component <ε_2> represents the amount of light absorption in the material [25].

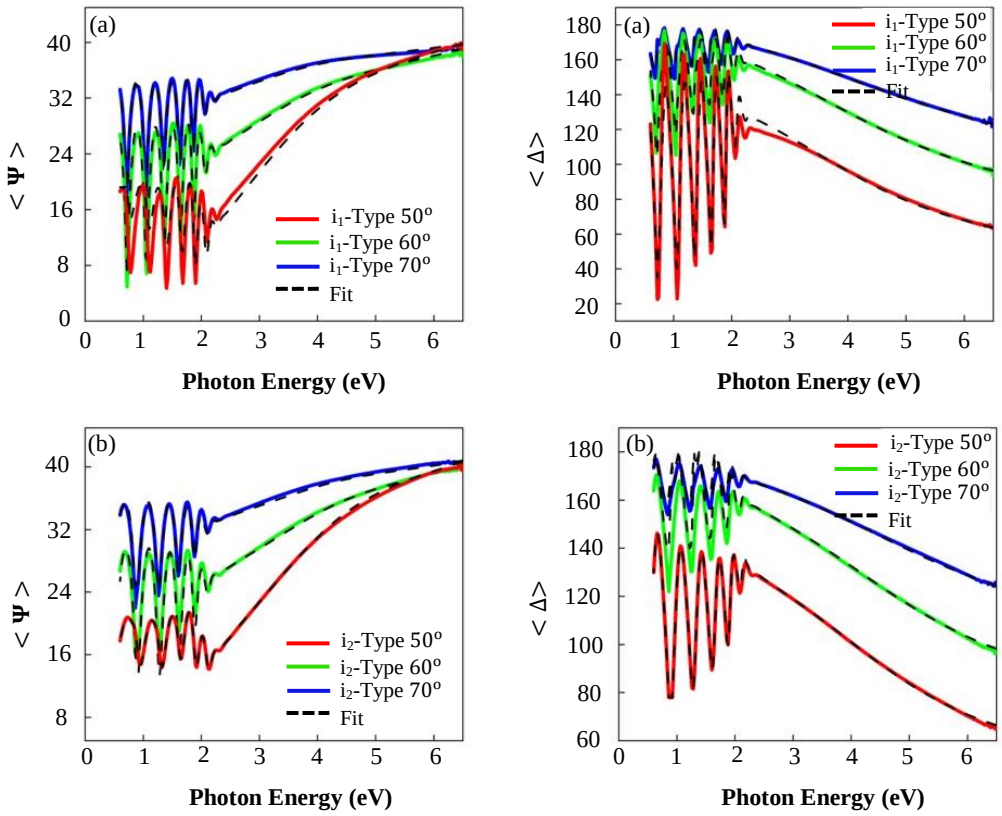

Figure 3 Real and imaginary part fitting model (a) i_1-type and (b) i_2-type of the values of ψ and Δ measured in SE with an angle of 50°, 60° and 70°

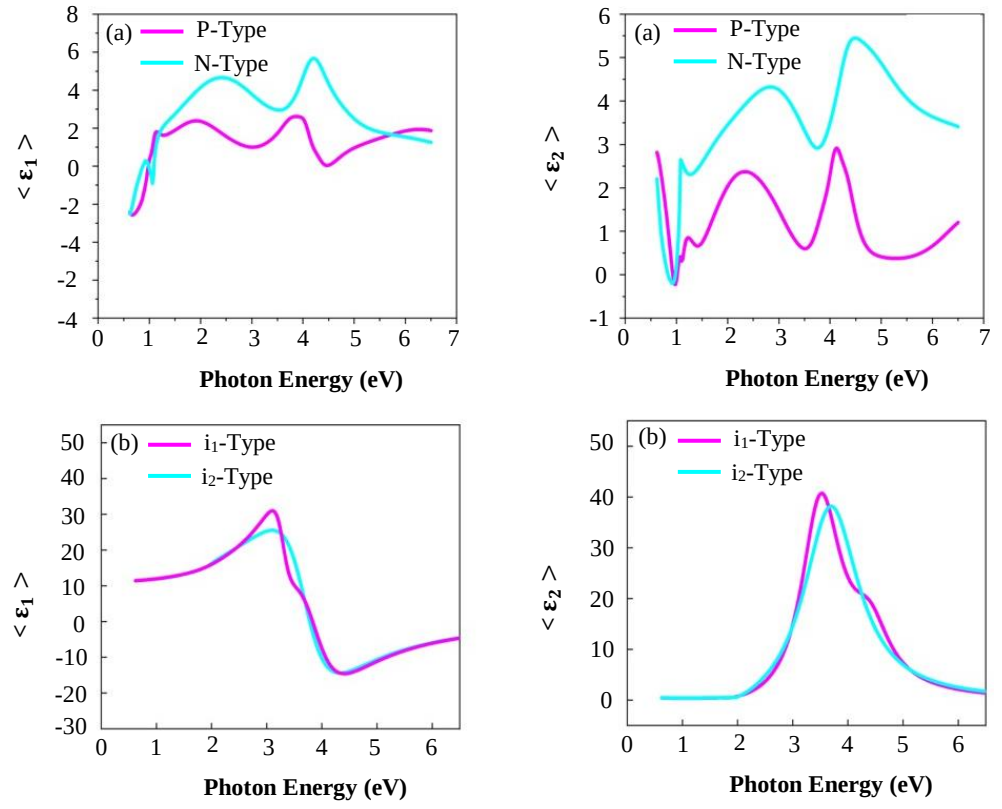

Figure 4 Dielectric function (a) p-type and n-type, (b) i_1-type and i_2-type. The real part <ε_1>, and (b) the imaginary part <ε_2>

Our results show that from the SE measurements it is obtained that the addition of an active layer (i-layer) can increase the dilution of hydrogen, not only the total hydrogen content in the film increases but the number of hydrogen bonds as strong Si-H also increases. The band gap increases because the Si-H bond has a higher energy than the Si-Si bond and the valence band is lower on the film. Figure 4 shows the addition of the active layer (i-layer) increases the energy gap with the total hydrogen content in the film. It is known that the energy gap increases almost linearly with the total hydrogen content. The increase in hydrogen content can be understood as follows: During the processing of hydrogen plasma, a small part of the amorphous phase is carved out and an nc-Si seed layer is formed.

The measured values of the dielectric constant as a function of photon energy are installed using TL + BEMA, namely the parameter values assigned to A, E_0, C and Eg are listed in Table 3 and the corresponding roughness, energy gap and bias values are listed in Table 4. The values calculated from the fraction amorphous, crystalline, and void for bulk and coarse surface layers are listed in Table 4 along with roughness values obtained from AFM [26, 27]. As can be seen from this table, there is a good fit between the values of A, E_0, C and Eg in the model TL + BEMA. The amplitude parameter value (A) was found to increase and the expansion parameter (C) decreased with increasing plasma H_2 dilution (Table 3). These observations indicate an increase in structural order with H_2 dilution. It was also observed that the volume fraction of the amorphous and void phases decreased and the crystalline phase increased with increasing plasma hydrogen phase (Figure 4). The thickness, energy and refractive index calculated using this model also corresponden to the values obtained from the UV-VIS transmission data. The film roughness of the AFM study was also very similar to the thickness of the rough surface layer (Figure 5).

Table 3 Model fitted parameters (A, E_0, C and Eg) of p-type, n-type, i_1-type and i_2-type films.

Layer	TL + BEMA Model			
	A (eV)	E_o (eV)	C (eV)	E_g (eV)
p-type	225 ± 1.35	3.40 ± 0.01	3.5 ± 0.01	2.00 ± 0.01
n-type	225 ± 1.35	3.38 ± 0.01	3.5 ± 0.01	1.95 ± 0.01
i_1-type	230 ± 1.20	3.40 ± 0.01	3.2 ± 0.01	1.65 ± 0.01
i_2-type	235 ± 1.20	3.40 ± 0.01	3.4 ± 0.01	1.84 ± 0.01

Table 4 Void, amorphous and crystalline fraction of bulk and surface roughness layer of p-type, n-type, i_1-type and i_2-type films calculated from SE and RMS roughness from AFM measurements.

Layer	Bulk layer			Surface roughness layer			AFM
	f_v (%)	f_a (%)	f_c (%)	f_v (%)	f_a (%)	f_c (%)	Roughness (nm)
p-type	6.43 ± 0.12	42.57 ± 1.54	39.5 ± 2.72	13.4 ± 0.58	50.2 ± 2.01	39.4 ± 1.25	8.95 ± 0.2
n-type	8.32 ± 0.18	62.34 ± 3.01	16.7 ± 1.01	25.3 ± 0.65	63.8 ± 2.67	14.5 ± 1.08	7.45 ± 0.3
i_1-type	9.44 ± 0.22	83.06 ± 3.86	4.22 ± 0.28	31.4 ± 0.86	65.5 ± 2.88	4.10 ± 0.59	5.60 ± 0.2
i_2-type	9.44 ± 0.22	83.06 ± 3.86	4.22 ± 0.28	31.4 ± 0.86	65.5 ± 2.88	4.10 ± 0.59	6.20 ± 0.2

Measurement of the thickness and morphology of the sample using AFM will characterize the material using atomic forces between the tip and the substrate. AFM consists of several devices such as tip, cantilever, piezoelectric sensor and photo-detector [28]. During the material characterization process, the tips move along the surface of the test material, causing the cantilever's slope to vary. The cantilever slope is detected by the photo-detector. The laser beam given to the cantilever is received by the detector which is detected as the cantilever slope. Measurements or scanning are taken at the layer and substrate boundary area (no layer). Scanning on this border area information on the difference in height or depth which states the thickness of the thin layer formed.

The results of measurements using AFM for each layer of p-type, n-type, type-i_1, and type-i_2 are as shown in Figure 5. In the measurement results, the surface roughness of the coating shows the surface morphology of the p-type, n-type, i_1 and type-i_2 layers in a layer area of 2x2 μm^2. Here it is found that the p-type, n-type, i_1-type, and i_2-type layers are very uniform across layers. The small grain size was clearly observed in all layers. It is caused by changes in nucleation and growth process in layers using PECVD. Surface roughness value *Root-Mean-Square* (RMS) of each of the p-type layer, n-type, i_1-type and i_2-type obtained from AFM measurements found 8.95 nm, 7.45 nm, 5.60 nm and 6:20 nm. From this very good roughness value, it can increase the occurrence of electron transport in each layer of the solar cell a-Si: H.

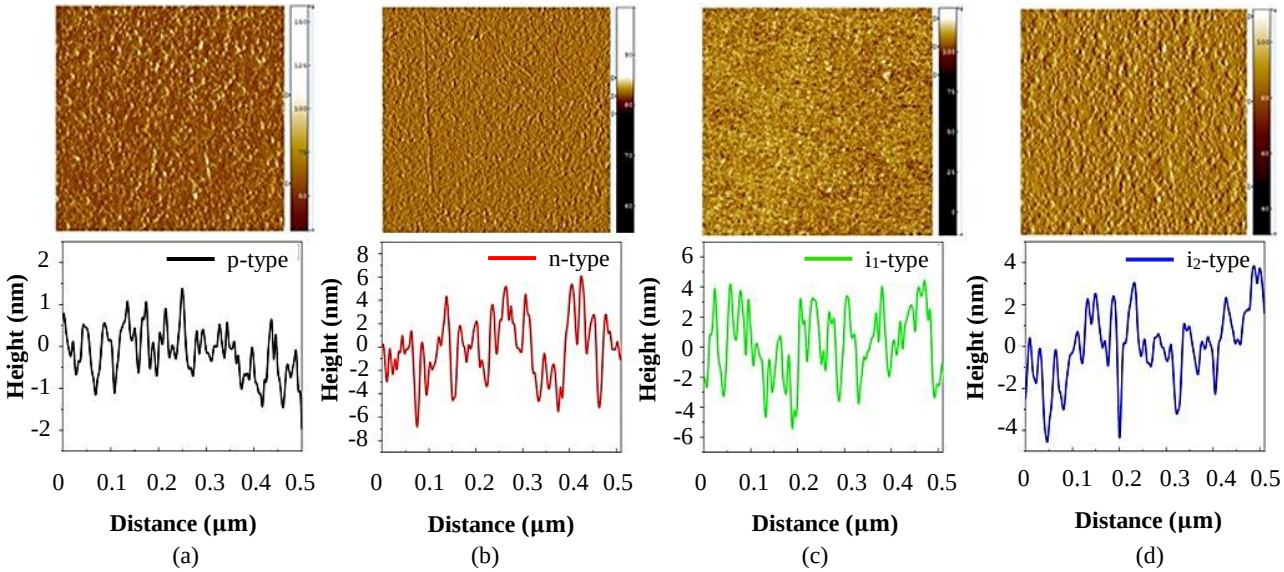

Figure 5 Surface morphology and thickness. (a) p-type, (b) n-type, (c) i_1-type, and (d) i_2-type.

The results of the characterization of solar cells a-Si: H sample p-i_1-i_2-n and sample p-i_2-i_1-n were measured using the *Keithley 617* solar simulator. Figure 6 shows the results of measurement of I-V characteristics of solar cells a-Si: H is generated in the sample p-i_1-i_2-n and sample p-i_2-i_1-n. One of the factors that caused the low fill factor value of the solar cells a-Si: H sample p-i_1-i_2-n and sample p-i_2-i_1-n produced was the imperfect joint formation mechanism that created defect conditions in the interlayer area (interface).

It is known that the solar cells a-Si: H sample p-i_1-i_2-n and sample p-i_2-i_1-n five junction regions. Each of these is a connection between the ITO substrate and the p-layer, between the p-layer and the i_1-layer, between the i_1-layer and the i_2-layer, between the i_2-layer and the n-layer, and between the n-layer and metal contacts. If the connection between these layers is not formed properly it will create defect conditions in the joint area [29, 30]. The defects formed in each junction will also contribute greatly to the increase in the value of the series resistance of the solar cells a-Si: H sample p-i_1-i_2-n and sample p-i_2-i_1-n. If this happens, the current generated by the irradiation effect (*photo-current*) will decrease rapidly with increasing bias voltage.

To observe changes in the work function of the front contact between ITO/(p)a-Si:H, it is depicted by the change in the front contact barrier height (φ_{b0}) by taking a variation of the typical front work function (WF_{TCO}) values based on experimental results, namely 5.20 eV (φ_{b0} = 1.42 eV), 5.42 eV (φ_{b0} = 1.62 eV), and 5.66 eV (φ_{b0} = 1.68 eV), respectively [31-33]. Meanwhile, the neutral back contact barrier height (φbL), at the n/metal interface is kept constant at a value of 0.2 eV (~ WB_{TCO} = 4.0 eV). Based on the typical φ_{b0} parameter, the effect of front barrier height will be tested on changes in doping concentration, bandgap, and thickness of the p-window layer. Other parameters used in the simulation referred to the Table 5.

The expression used to describe the relationship between work functions (front and back contact) refers to Figure 6 are $WF_{TCO} = \varphi_{b0} + \chi_{at\ x=0}$ and $WB_{TCO} = \varphi_{bL} + \chi_{at\ x=L}$, where WF_{TCO}, WF_{TCO}, φ_{b0}, φ_{bL}, $\chi_{at\ x=0}$, $\chi_{at\ x=L}$ are the front work function, the back work function, the front contact barrier height, the back contact barrier height, the front electron affinity, and the back electron affinity [34, 35]. From Figure 7 by referring to the geometric structure in the energy diagram of the p-i_1-i_2-n solar cell structure, another relationship can be derived to express the quantities φ_{b0}dan φ_{bL}, as follows:

$$\varphi_{b0} = E_G\,(p) - E_{act}\,(p) - E_{sbb} \tag{2}$$

$$\varphi_{bL} = E_C - E_F = E_{act}\,(n) \tag{3}$$

where $E_G\,(p)$, $E_{act}(p)$, E_{sbb} , E_C , E_F , $E_{act}(n)$ are the mobility band gap of the (p) a-Si:H layer, the activation energy of the (p) a-Si: H layer, surface band bending, the conduction band, the Fermi energy, and the activation energy of the (n) a-Si:H layer.

Table 5 Parameters input for simulated of the p-i_1-i_2-n solar cell using AFORS-HET

Parameters	(p)a-Si:H	(i_1)a-Si:H	(i_2)a-Si:H	(n)a-Si:H
Layer thickness (nm)	15	100-500	100-500	25
Dielectric constant	11.9	11.9	11.9	11.9
Electron affinity (eV)	3.8	3.80	3.80	3.80
Band gap (eV)	2.0	1.7-1.86	1.7-1.86	2.2
Effective cond. band density (cm^{-3})	2.5×10^{20}	2.5×10^{20}	2.5×10^{20}	2.5×10^{20}
Effective val. band density (cm^{-3})	2.5×10^{20}	2.5×10^{20}	2.5×10^{20}	2.5×10^{20}
Acceptor concentration, Na (cm^{-3})	3.0×10^{18}	0	0	0
Donor concentration, Nd (cm^{-3})	0	0	0	1.0×10^{19}
Electron mobility ($cm^2V^{-1}s^{-1}$)	10	20	20	10
Hole mobility ($cm^2V^{-1}s^{-1}$)	1	2	2	1
Thermal velocity of electron (cms^{-1})	1.0×10^{7}	1.0×10^{7}	1.0×10^{7}	1.0×10^{7}
Thermal velocity of hole (cms^{-1})	1.0×10^{7}	1.0×10^{7}	1.0×10^{7}	1.0×10^{7}
Defect density at conduction (valence) band edge ($cm^{-3}eV^{-1}$)	6.67×10^{20} (6.67×10^{20})	2.33×10^{21} (2.33×10^{21})	2.0×10^{21} (2.0×10^{21})	2.0×10^{21} (2.0×10^{21})
Urbach energy for conduction (valence) band tail (eV)	0.03(0.06)	0.03(0.06)	0.03(0.06)	0.03(0.06)
Capture cross section σ_e (σ_h) for conduction band tail (cm^2)	1.0×10^{-17} (1.0×10^{-15})	1.0×10^{-17} (1.0×10^{-15})	1.0×10^{-17} (1.0×10^{-15})	1.0×10^{-17} (1.0×10^{-15})
Capture cross section σ_e (σ_h) for valence band tail (cm^2)	1.0×10^{-15} (1.0×10^{-17})	1.0×10^{-15} (1.0×10^{-17})	1.0×10^{-15} (1.0×10^{-17})	1.0×10^{-15} (1.0×10^{-17})
Gaussian density of states (cm^{-3})	8.0×10^{17}	8.0×10^{15}	8.0×10^{15}	8.0×10^{17}
Gaussian peak energy for donor(acceptor) (eV)	1.22(0.70)	1.22(0.70)	1.22(0.70)	1.22(0.70)
Standard deviation of Gaussian for donor (acceptor) (eV)	0.23(0.23)	0.23(0.23)	0.23(0.23)	0.23(0.23)
Capture cross section σ_e (σ_h) for donor-like Gaussian States (cm^2)	1.0×10^{-14} (1.0×10^{-15})	1.0×10^{-14} (1.0×10^{-15})	1.0×10^{-14} (1.0×10^{-15})	1.0×10^{-14} (1.0×10^{-15})
Capture cross section σ_e (σ_h) for acceptor-like Gaussian states (cm^2)	1.0×10^{-15} (1.0×10^{-14})	1.0×10^{-15} (1.0×10^{-14})	1.0×10^{-15} (1.0×10^{-14})	1.0×10^{-15} (1.0×10^{-14})

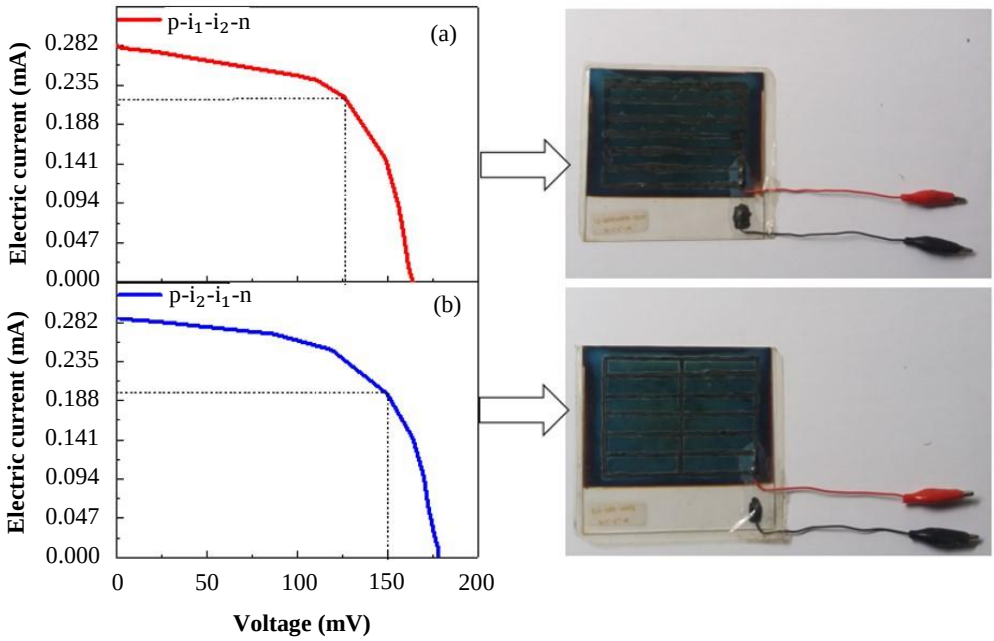

Figure 6 Efficiency of solar cells a-Si: H. (a) sample p-i$_1$-i$_2$-n 7.79%, and (b) sample p-i$_2$-i$_1$-n 8.49%.

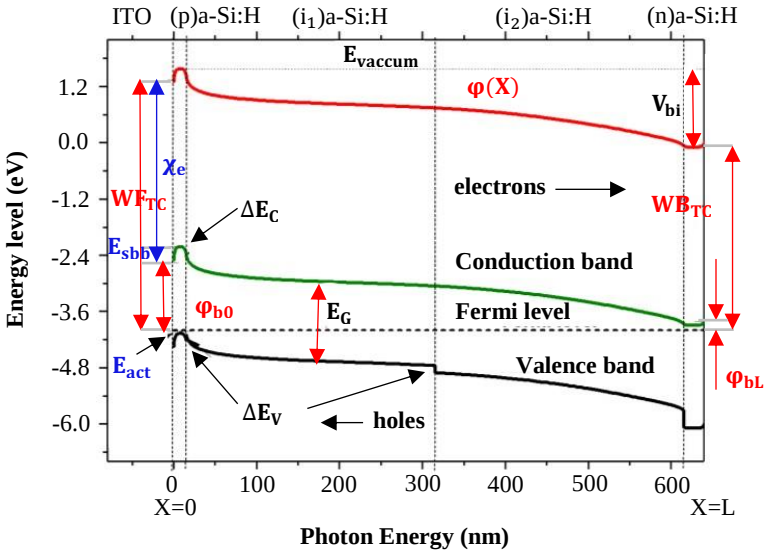

Figure 7 Simulated band diagram of the p-i$_1$-i$_2$-n solar cell at thermodynamics equilibrium generated by AFORS-HET simulator

4. Conclusion

Based on the results obtained in this study, it was reported that the effect of active layer thickness on the performance of amorphous hydrogenated silicon solar cells (a-Si: H) obtained a fairly good increase in conversion efficiency with an increase in efficiency of 7.79% in the p-i$_1$-i$_2$-n sample to 8.49% for the p-i$_2$-i$_1$-n sample. The conversion efficiency of solar cells produced with the thickness of the active layer (i-layer) is still very possible to be improved, among others, such as adding back contact as an optical enhancement factor, marked by the increase in light absorption by the a-Si: H layer. The optical enhancement factor is the average distance of light before it is absorbed by the a-Si: H layer, it occurs because the light is reflected by the back contact.

The conversion efficiency of solar cells produced by the addition of the active layer (i-layer) is still possible to improve, among others, such as insertion of a buffer layer in the areas between layers, the use of p-layer with doping-delta (δ-doped) which is proven to be able to improve the performance of a-Si: H solar cells with a uniform doping p-layer, the use of a-SiC: H material in the p-layer which is known to be more transparent than a-Si: H, or the use of a tandem structure (a-Si: H based pin solar cell for upper cells connected with p-i-n solar cells based on μc-Si: H for bottom cells).

5. Acknowledgements

One of the authors (SP) thankfully acknowledges the Ministry of Finance of the Republic of Indonesia, through the Lembaga Pengelolah Dana Pendidikan (LPDP), which has provided financial support through the Scholarship Indonesian. The authors would also appreciate LPPM Institut Teknologi Sepuluh Nopember for the use of experimental facilities at Research Center ITS. We are thankful to Prof. Andrivo Rusydi who provided a fruitful discussion for this paper.

6. References

[1] Prayogi S, Cahyono Y, Iqballudin I, Stchakovsky M, Darminto D. The effect of adding an active layer to the structure of a-Si:H solar cells on the efficiency using RF-PECVD. J Mater Sci Mater Electron. 2021;32(6):7609-18.
[2] Fritzsche H. A new perspective on an old problem: the Staebler-Wronski effect. MRS Online Proc Libr. 2009;1245:1401.
[3] Wagner D, Irsigler P. On the annealing behaviour of the Staebler-Wronski effect ina-Si:H. Appl Phys A Solid Surface. 1984;35(1):9-12.
[4] Watts C, Aspitarte L, Lin Y, Li W, Elzein R, Addou R, et al. Light soaking in metal halide perovskites studied via steady-state microwave conductivity. Comm Phys. 2009;3(1):73-882.
[5] Sadatgol M, Bihari N, Pearce JM, Guney DO. Scalable honeycomb top contact to increase the light absorption and reduce the series resistance of thin film solar cells. Opt Mater Express. 2014;9(1):256-68.
[6] Dehghanifard Z, Ahmadi AR, Ganjovi AR. Space-time coupled finite element simulation of PECVD reactor. Int J Appl Comput Sci Math. 2017;2(3):303-13.
[7] Droes SR, Kodas TT, Hampden-Smith MJ. Plasma-enhanced chemical vapor deposition (PECVD). In: Weimer AW, editor. Carbide, Nitride and Boride Materials Synthesis and Processing. Dordrecht: Springer; 2011. p. 579-603.
[8] Moiseev T, Chrastina D, Isella G. Plasma composition by mass spectrometry in a Ar-SiH_4-H_2 LEPECVD process during nc-Si deposition. Plasma Chem Plasma Process. 2017;31(1):157-74.
[9] Pham DP, Kim S, Park J. Reduction in photocurrent loss and improvement in performance of single junction solar cell due to multistep grading of hydrogenated amorphous silicon germanium active layer. Silicon. 2011;10:759-67.
[10] Kabir MI, Shahahmadi SA, Lim V, Zaidi S, Sopian K, Amin N. Amorphous silicon single-junction thin-film solar cell exceeding 10% efficiency by design optimization. Int J Photoenerg. 2012;2012:460919.
[11] Parashar D, Krishna VSG, Moger SN, Keshav R, Mahesha MG. Thickness optimization of ZnO/CdS/CdTe solar cell by numerical simulation. Trans Electr Electron Mater. 2019;21:587-93.
[12] Massiot I, Cattoni A, Collin S. Progress and prospects for ultrathin solar cells. Nat Energ. 2018;5(12):959-72.
[13] Prompan P, Wongkhan K, Jitchati R. Co-sensitized ruthenium(II) for dye-sensitized solar cells (DSSCs). KKU Eng J. 2006;43(S1):133-6.
[14] Wongcharee K, Udomman T, Meeyoo V, Suttakat K, Sangphookhei T. Preparation of platinum-free tubular dye-sensitized solar cells by electrophoretic deposition. KKU Eng J. 2016;43(4):178-83.
[15] Hussain I, Tran HP, Jaksik J, Moore J, Islam N, Uddin M. Functional materials, device architecture, and flexibility of perovskite solar cell. Emergent Mater. 2015;1:133-54.
[16] Prayogi S, Ayunis, Kresna, Cahyono Y, Akidah, Darminto D. Analysis of thin layer optical properties of a-Si:H P-type doping CH_4 and P-Type without CH_4 is deposited PECVD systems. J Phys Conf Ser. 2017;853(1):012032.
[17] Muhammad MH, Hameed MFO, Obayya SS. Broadband absorption enhancement in periodic structure plasmonic solar cell. Opt Quant Electron. 2007;47(6):1487-94.
[18] Turapra P, Kaewrawang A, Tonmitra K. Study of mirror uses on electricity generation of solar cell. KKU Eng J. 2016;43(S1): 141-3.
[19] Prayogi S, Baqiya M, Cahyono Y, Darminto D. Optical transmission of P-Type a-Si:H thin film deposited by PECVD on ITO-coated glass. Mater Sci Forum. 2019;996:72-6.
[20] Frey H. Chemical vapor deposition (CVD). In: Frey H, Khan HR, editors. Handbook of thin-film technology. Berlin: Springer; 2002. p. 225-52.
[21] Cahyono Y, Yahya E, Zainuri M, Pratapa S, Darminto D. Quantum confinement in an intrinsic a-Si:H thin film deposited on soda lime glass substrate using PECVD. Trans Electr Electron Mater. 2017;19(1):69-73.
[22] Franta D, Necas D, Zajickova L, Ohlidal I, Stuchlik J. Advanced modeling for optical characterization of amorphous hydrogenated silicon films. Thin Solid Films. 2018;541:12-6.
[23] Hilfiker JN. 5-In situ spectroscopic ellipsometry (SE) for characterization of thin film growth. In: Koster G, Rijnders G, editors. In Situ Characterization of Thin Film Growth. Cambridge: Woodhead Publishing; 2011. p. 99-151.
[24] Oates TWH, Wormeester H, Arwin H. Characterization of plasmonic effects in thin films and metamaterials using spectroscopic ellipsometry. Progr Surf Sci. 2017;86(11-12):328-76.
[25] Stradins P, Teplin CW, Young DL, Yan Y, Branz HM, Wang Q. Crystallization of thin-film Si monitored in real time by in-situ spectroscopic techniques. J Mater Sci Mater Electron. 2016;18:309-13.
[26] Ahmad G, Das G, Roy JN. Performance and stability improvement of single junction a-Si:H solar cell by interface engineering. J Mater Sci Mater Electron. 2019;30(13):12406-15.
[27] Seba HY, Hadjersi T, Zebbar N, Brighet A, Berouaken M, Manseri A, et al. Alternating current impedance spectroscopic investigation of an a-Si:H/c-Si heterojunction with porous silicon multilayers. Thin Solid Films. 2011;699:137891.
[28] Kumar Saha J, Ohse N, Hamada K, Matsui H, Kobayashi T, Jia H, et al. Fast deposition of microcrystalline Si films from SiH_2Cl_2 using a high-density microwave plasma source for Si thin-film solar cells. Sol Energ Mater Sol Cell. 2017;94(3):524-30.
[29] Kanneboina V, Madaka R, Agarwal P. Spectroscopic ellipsometry studies on microstructure evolution of a-Si:H to nc-Si:H films by H2 plasma exposure. Mater Today Comm. 2012;15:18-29.
[30] Chakraborty M, Banerjee A, Das D. Spectroscopic studies on nanocrystalline silicon thin films prepared from H2-diluted SiH4-plasma in inductively coupled low pressure RF PECVD. Phys E Low-dimensional Syst Nanostruct. 2017;61:95-100.
[31] Abadias G, Chason E, Keckes J, Sebastiani M, Thompson GB, Barthel E, et al. Review article: stress in thin films and coatings: current status, challenges, and prospects. J Vac Sci Technal. 2019;36(2):020801.
[32] Shao S, Loi MA. The role of the interfaces in perovskite solar cells. Adv Mater Interfac. 2014;7(1):1901469.
[33] van Dyk EE, Meyer EL. Analysis of the effect of parasitic resistances on the performance of photovoltaic modules. Renew Energ. 2016;29(3):333-44.
[34] Kind R, van Swaaij RV, Rubinelli FA, Solntsev S, Zeman M. Thermal ideality factor of hydrogenated amorphous silicon p-i-n solar cells. J Appl Phys. 2009;110:104512.
[35] Kosyachenko LA. Possibilities to decrease the absorber thickness reducing optical and recombination losses in CdS/CdTe solar cells. Mater Renew Sustain Energ. 2018;2:14-55.